Veröffentlichung

Im Rahmen des SFB 880. www.sfb880.tu-braunschweig.de

Autoren

Rossian, Lennart;Suryadi, Alexandre;Rossignol, Karl-Stephane;Ewert, Roland;Herr, Michaela;Delfs, Jan;Kumar, Pradeep

Titel

Numerical and Experimental Insights into the Noise Generation of a Circulation Control Airfoil

Publisher o. Konferenz

AIAA AVIATION Conference 2018, Atlanta, USA

Jahr

2018

Internet-Link (Doi-Nr.)

Numerical and Experimental Insights into the Noise Generation of a Circulation Control Airfoil

L. Rossian* , A. Suryadi† , K.-S. Rossignol ‡ , R. Ewert§ , M. Herr¶ and J. W. Delfs‖
German Aerospace Center (DLR), D-38108 Braunschweig, Germany
P. Kumar**
Institute for Fluid Mechanics, TU Braunschweig, Germany

With the advances in reduction of propulsion related noise from aircraft, airframe noise gets more and more into focus. During approach and landing, the high-lift system of the wings becomes one major acoustic source region contributing to the overall emitted noise. One promising approach to reduce this airframe noise is to change the complete high-lift system from a classic three element slat-wing-flap configuration to a slit-less system with active blowing and droop nose. Preceding experimental investigations have shown, that such a configuration may provide a noise reduction above 2 kHz on the model scale. In the present abstract both numerical and experimental investigations concerning the acoustics of a high-lift wing with droop nose and active blowing are presented. Thereby, an insight into the acoustic source mechanisms is provided that will serve as a basis for the design of a low-noise high-lift configuration in the future.

Nomenclature

A	=	wing area [m^2]
b	=	wing span [m]
c	=	chord length [m]
c_μ	=	jet momentum coefficient
h	=	hight [m]
Ma	=	Mach number
p	=	pressure [Pa]
Re	=	Reynolds number
U	=	scalar velocity magnitude $\left[\frac{\mathrm{m}}{\mathrm{s}}\right]$
u	=	velocity in x-direction $\left[\frac{\mathrm{m}}{\mathrm{s}}\right]$
v	=	velocity in y-direction $\left[\frac{\mathrm{m}}{\mathrm{s}}\right]$
α	=	angle of attack [°]
ρ	=	density $\left[\frac{\mathrm{kg}}{\mathrm{m}^3}\right]$
σ	=	relaxation parameter
ω	=	vorticity $\left[\frac{1}{\mathrm{s}}\right]$

Superscripts

*PhD Student, Technical University Braunschweig, corresponding author lennart.rossian@dlr.de
†Research Scientist, AIAA Member
‡Research Scientist, Senior AIAA Member
§Senior Scientist, Senior AIAA Member
¶Senior Scientist, Senior AIAA Member
‖Head of Technical Acoustics Department, DLR Institute of Aerodynamics and Flow Technology, Professor for Technical Acoustics at TU Braunschweig, Senior AIAA Member
**PhD Student, Technical University Braunschweig

0 = mean flow quantity
$'$ = fluctuating acoustic quantity

Subscripts

AWB = Acoustic Windtunnel Braunschweig
∞ = far field quantity
jet = blowing jet quantity
MUB = Modell Unterschallwindkanal Braunschweig
$slit$ = jet slit geometry

I. Introduction

The aim of the collaborated research center SFB880 is to investigate concepts for high lift devices for future commercial aircraft. Therein, both aerodynamic and aeroacoustic analysis is carried out to meet performance and noise requirements. One promising approach to such low-noise high-lift devices are circulation control airfoils with high flap deflection angles as sketched in figure 1. These go without slotted slats and flaps and are able to provide very high lift coefficients. To avoid flow separation due to the strongly bend flow, a high speed tangential blowing is realized on the flap. This effect was first described by Coanda[1] and has since been successfully simulated and tested in wind tunnels[2] as well as flight demonstrators.[3]

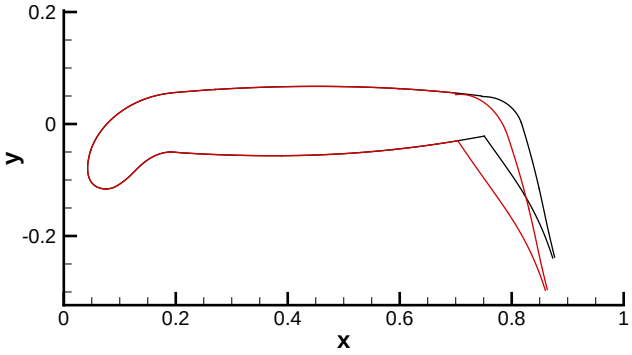

Figure 1: The two different airfoil geometries used for simulation (black) and measurement (red).

In 2010, Pott-Pollenske and Pfingsten[4] showed experimentally that with such a circulation control airfoil significant noise reduction in the frequency range of 2 to 20 kHz on model scale can be achieved compared to a classic 3 element high lift airfoil with slotted slat and flap. However, in the lower frequency domain a noise increase was found. This might be related to installation effects.

An analytical approach to break down the acoustic sources of a circulation control wing by Howe[5] revealed four principle source mechanisms:

- interaction of jet turbulence with the jet slot
- interaction of the exterior turbulent boundary layer with the jet slot
- curvature noise at the rounded behind the jet slot
- separation noise at the trailing edge

Note, that this analysis was carried out for an airfoil without flap but with a rounded trailing edge. Therefore, transfered to the configuration in the present work, the separation noise will be replaced by classic trailing edge noise and the large separation bubble at the kink of the pressure side of the flap needs to be considered.

For the present work, both numerical as well as experimental investigations were performed on circulation control airfoils with a droop nose that are based on DLR's F16 airfoil. It has to be noted that the results in this abstract are based on two different configurations that are shown in figure 1. For the experimental investigations, the airfoil was equipped with a longer flap than for the numerical simulations, while the flap

deviation angle was constant. Therefore, the results are not yet directly comparable. However, the principle phenomena related to noise generation are supposed to be the same, so that a qualitative comparison is feasible. For the final paper the numerical simulations of the experimentally tested configuration will be completed.

II. Numerical Setup

To simulate the noise radiated from an airfoil with blowing for circulation control the hybrid two-step CFD/CAA procedure including DLR's CAA Code PIANO is used. Therefore, in a first step an unsteady RANS CFD computation is run. From the result a time-averaged flow field is derived which provides the mean flow and the turbulence statistics. In the CAA step the Linearized Euler Equations (LEE) are solved atop this mean flow. Therefore, the acoustic sources are provided by the fast Random Particle Mesh method (fRPM) by reconstruction of the turbulent vortices based on the turbulence statistics provided by the CFD. In the following sections the basic input for the CAA computations is presented before going into detail about the considered acoustic source mechanisms.

II.A. CAA Mesh and Mean flow

DLR's CAA code PIANO solves the perturbation equations on a block structured mesh. The general topology of the 2D mesh can be seen in figure 2 along with different source regions that are presented later in section II.B.2. The mesh is set to resolve frequencies up to 15 kHz with 7 points per wavelength. Due to necessary refinements inside the source regions frequencies up to 30 kHz are resolved on a circle with the radius of one chord length around the flap trailing edge. For the region of the blowing at the flap the mesh needs special refinement to resolve the jet that exits through a nozzle of 0.2 mm and reaches a local Mach number of up to 1.1.

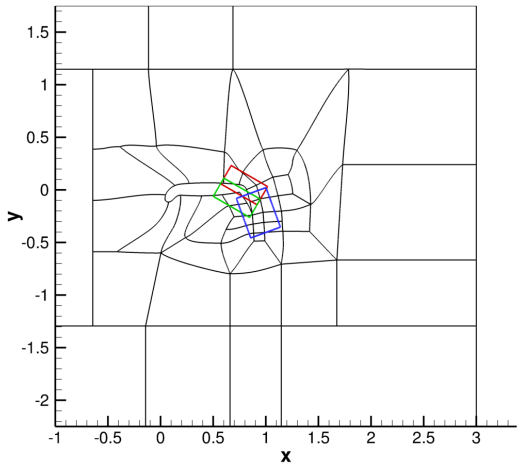

Figure 2: Block structure of the CAA mesh with fRPM source regions marked by the colored blocks.

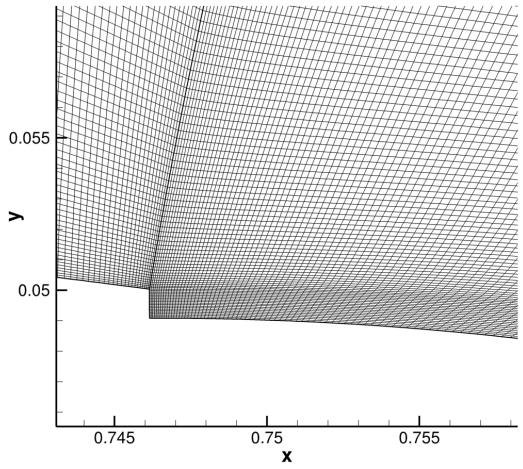

Figure 3: Detail of the mesh refinement in the jet area.

Figures 4 and 5 show the state of the mean flow, provided by the Institute for Fluid Mechanics of TU Braunschweig, around the airfoil by the local Mach number and selected streamlines. It is calculated for a chord length of $c = 0.3\,\mathrm{m}$ at a free stream Mach number of $Ma_\infty = 0.151$, a Reynoldsnumber of $Re = 1 \cdot 10^6$ and an angle of attack of $\alpha = 15°$. Figure 5 illustrates nicely the effect of the wall jet that leads to an attached flow on the flap despite the large separation area of the boundary layer originating from the airfoil's suction side.

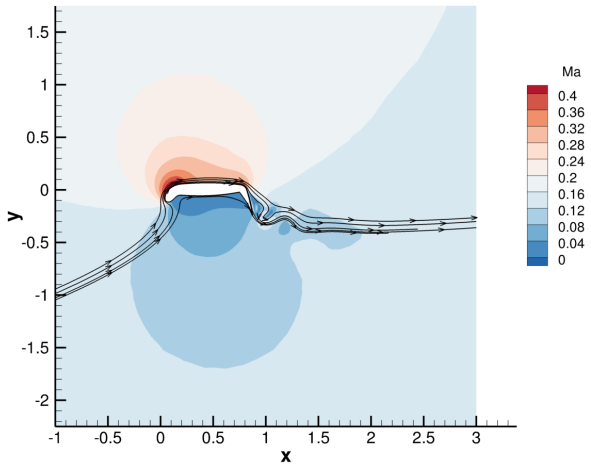

Figure 4: Mean flow around airfoil with local Mach number ($c = 0.3\,\mathrm{m}$, $Re = 1 \cdot 10^6$, $Ma_\infty = 0.15$, $\alpha = 15°$, $Ma_{jet} = 1.1$).

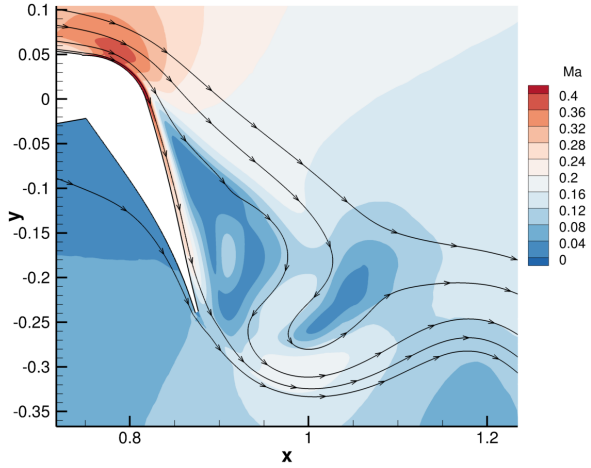

Figure 5: Detail of flow separation on the flap with attached wall jet.

II.B. Aeroacoustic Sources

In the following paragraphs the numerical approaches to model the relevant acoustic sources are presented. Thereby, two general source mechanisms are considered, both based on the fRPM method. On the one hand the jet mixing noise is based on the model formulated by Tam and Auriault.[6] On the other hand, an eddy relaxation source term formulated by Neifeld et al.[7] is used to account for turbulence induced noise interacting with the geometry of the airfoil. Both methods provide source terms that are directly used with the Linearized Euler Equations (LEE).

II.B.1. Jet Mixing Noise

The jet mixing noise source, that is related to turbulence-turbulence interaction, is modeled by the semi-empiric model formulated by Tam and Auriault[6] with a Langevin force that accounts for the temporal fluctuations. Note, that this model was initially formulated for round jets. However, Ahuja et al.[8] showed, that the Tam and Auriauld model is also applicable to high aspect ratio jets that are to be considered in the case of circulation control airfoils.

II.B.2. Turbulence-Geometry Interaction Noise

As described in section I, the jet mixing noise is only one acoustic source mechanism amongst others. Therefore, further simulations are carried out concentrating on interaction noise of turbulence with the airfoil. With the use of the fRPM method individual source locations can be investigated by placing the reconstruction domain in the respective region. Here, three areas are considered specifically corresponding to those listed in section I:

- the trailing edge of the flap (blue box in figure 2)
- the suction side of the flap with strongly curved flow and jet slot (red box in figure 2)
- the kink with detached flow on the pressure side of the flap (green box in figure 2)

The source mechanism is hereby represented by an eddy relaxation source term that is coupled to the Linearized Euler Equations. Figure 6 illustrates this approach that was formulated by Neifeld et al.[7] for the application of jet noise. Thereby, the turbulence reconstruction method fRPM is used to implement a 4D spatial and temporal vorticity source term by comparing the reconstruction to the vorticity calculated in the

CAA domain. The coupling is then realized by the relaxation parameter σ which is of order of magnitude of 10^{-4}.

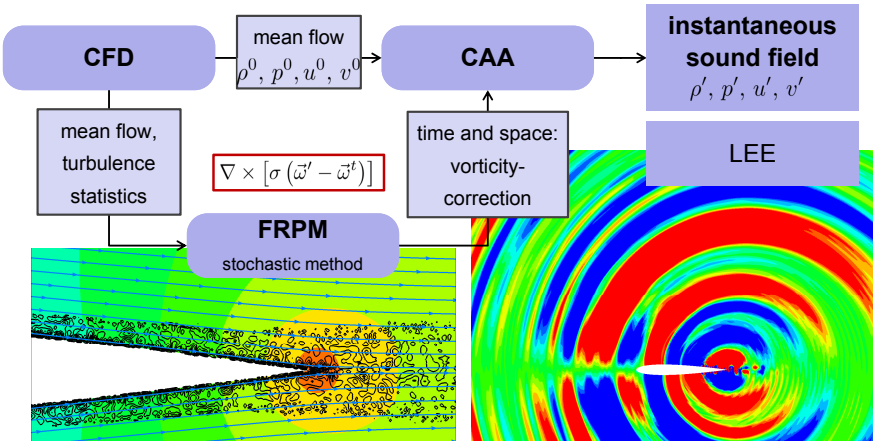

Figure 6: Flowchart of eddy relaxation source term of fRPM (fast Random Particle Mesh) turbulence reconstruction method in use with CAA code PIANO.[9]

III. Experimental Setup

Measurements were performed in the acoustic wind tunnel Braunschweig (AWB) at DLR Braunschweig, Germany. This wind tunnel has an open jet test section and a maximum speed of up to 65 $\frac{\text{m}}{\text{s}}$ with a turbulence intensity of up to 0.3%. It is designed to conduct acoustics measurements. The test section is covered by anechoic wedge foams to reduce ambient noise. A 2-axis movable collector limits the interaction of the jet shear layer with the walls of the test section.[10]

The nozzle of the wind tunnel is 0.8 m wide and 1.2 m high. Side walls were mounted to the nozzle to hold an airfoil model. The airfoil model that was used in this study was previously installed in the MUB wind tunnel in the Institute of Fluid Mechanics in the Technical University Braunschweig for aerodynamic measurements. The cross-sectional area of the MUB is larger than the nozzle area of the AWB. The model, based on the DLR F-16 profile, has an effective chord length of $c = 0.3$ m and spanwise length of $b = 1.3$ m. With droop nose and a 30%c flap deflected at 65°, the geometric chord length is 0.23 m.

Circulation control via high-speed jet was realized by a high-aspect ratio slit nozzle on the suction side ahead of the flap segment. The height of the slit $h_{slit} = 2 \times 10^{-4}$ m, and the slit width extends the full span width of the model $b_{slit} = 1.3$ m. The high-speed jet was actualized by feeding air from the sides of the airfoil from a compressor outside of the test section.

The model was installed horizontally and the span of the model where blowing is considered is 0.8 m. If left untreated, from the excess parts of the model the jet noise will contaminate the measurements. In the first attempt, the jet slit in the excess portions of the model were covered by aluminum tape, but the high pressure of the jet would always eventually tear them off. Because of that, the excess portion was minimized acoustically by foam covering, while airflow leakage was unavoidable.

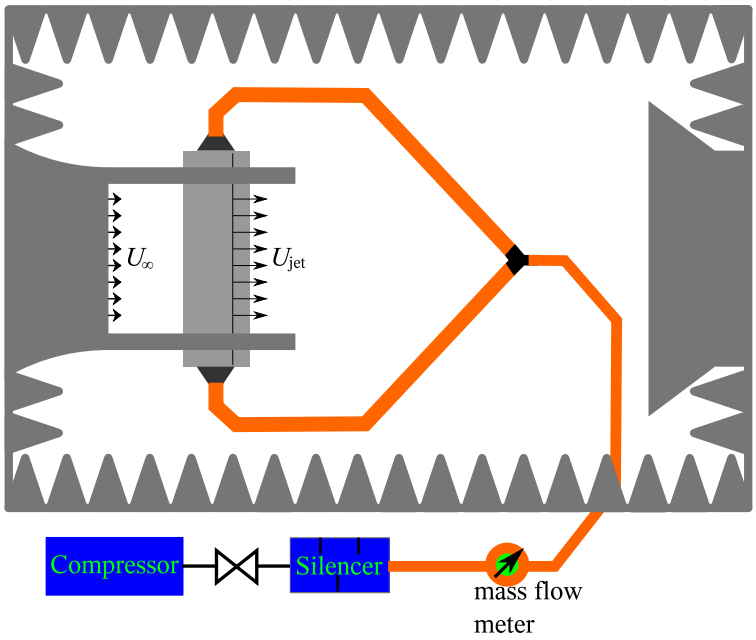

Figure 7: Experimental setup of the high speed jet for airfoil circulation control. Only the test section of the AWB is shown.

III.A. Correction of c_μ for Excess Jet

A mass flow meter monitors the flow of air going into the airfoil model, which also measures the jet momentum coefficient, $c_{\mu,meas}$. This magnitude has to be corrected for the excess jet slit. The measured $c_{\mu,meas}$ is defined as

$$c_{\mu,meas} = \frac{\dot{m} U_{jet}}{0.5 \rho_\infty U_\infty^2 A_{ref}} \tag{1}$$

where $\dot{m}$ is the mass flow as measured by the mass flow meter, $A_{ref} = 0.3$ m $\times 0.8$ m is the effective planform area of the model, which circulation is controlled, and U_{jet} is the jet velocity that is defined by interpolating

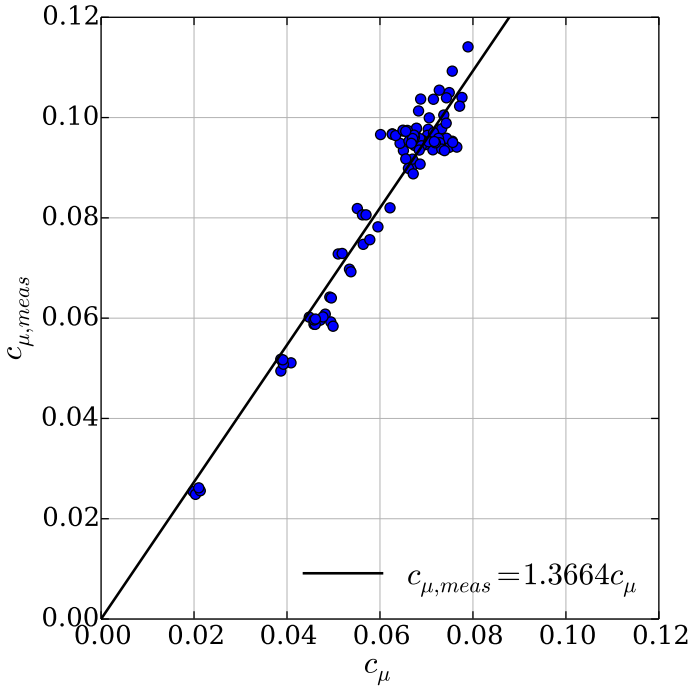

Figure 8: Linear regression between $c_{\mu,meas}$ and corrected c_μ.

Table 2: Correction table for c_μ.

$c_\mu, meas$	c_μ
0.060	0.044
0.090	0.066
0.095	0.069
0.100	0.073

the static pressure located at positions upstream and downstream of the jet slit. The calculation of U_{jet} is defined as

$$U_{jet} = 0.96 \left[\frac{2\gamma R_s T_{pl}}{\gamma - 1} \left(1 - \frac{P_{jet}}{P_{pl}} \right)^{\frac{\gamma-1}{\gamma}} \right]^{1/2} \tag{2}$$

where T_{pl} and P_{pl} are the temperature and static pressure measured in the plenum, respectively, $\gamma = 1.4$ is the adiabatic index, and $R_s = 287.058$ is the specific gas constant.

The measured mass flow, $\dot{m}$, is the sum of mass flow used for circulation control and mass flow from the excess parts. Mass flow of jet exiting the narrow slit is defined as $\dot{m} = \rho_{jet} U_{jet} h_{slit} b_{slit}$, substituting into equation (1) leads to

$$c_\mu = \frac{\rho_{jet} U_{jet}^2 b_{slit} h_{slit}}{0.5 \rho_\infty U_\infty^2 A_{ref}} \tag{3}$$

The jet momentum coefficient used for circulation control is a function of h_{slit}, b_{slit}, and ρ_{jet} compensated for compressibility by

$$\rho_{jet} = \rho_\infty \left(\frac{T_{jet}}{T_\infty} \right)^{\frac{1}{\gamma-1}} \tag{4}$$

The relation between $c_{\mu,meas}$ and c_μ in Eq. (5) is formulated by drawing a linear regression of the available data as shown in figure 8

$$c_{\mu,meas} = 1.3664 c_\mu \tag{5}$$

The measured and corrected values are shown in table 2. Boundary layer reattachment on the flap segment was observed in the AWB when $c_\mu = 0.066$. This value was reported in the MUB as $c_\mu = 0.062$, which is an acceptable variation of 6.4%.

III.B. Aerodynamic measurements

The model is equipped with 63 static pressure ports to measure the pressure coefficients of the model at $\alpha_{AWB} = 6°$ and 11° that are equivalent to $\alpha_{MUB} = 0°$ and 5°, respectively. These angles were selected to have comparable pressure coefficients with measurements that were performed in the MUB. The comparison is judged good when the pressure coefficients on the flap segment from AWB and MUB overlap each other. The two sets of pressure coefficients are shown in figure 9.

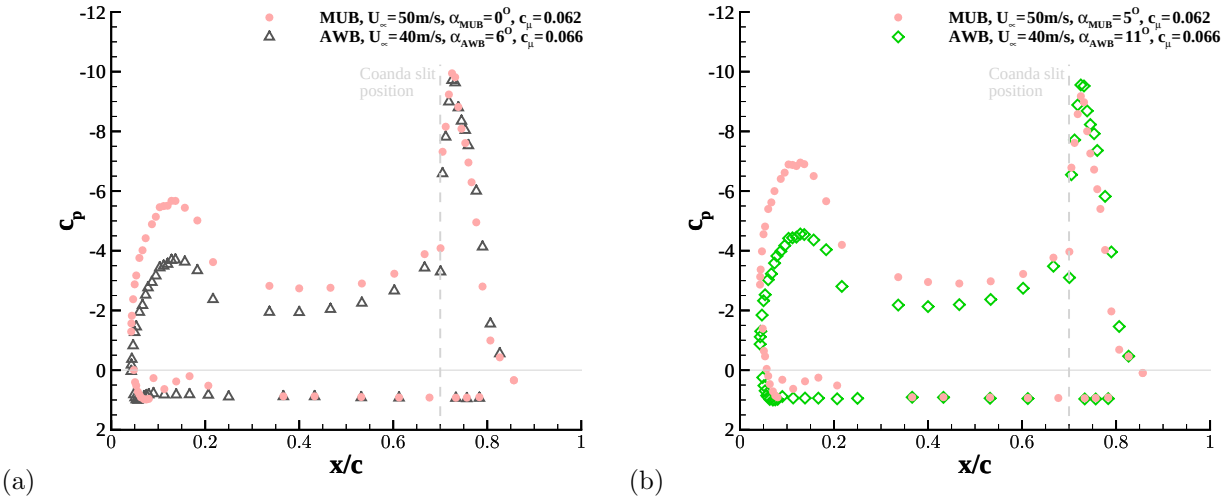

(a) (b)

Figure 9: Coefficient of pressure for c_μ of boundary layer reattachment for $\alpha_{AWB} = 6°$ and 11°.

III.C. Acoustic Measurements

Three acoustic measurement systems were used in this study. Far-field microphones, a large aperture microphone array with 96 microphones, and a small aperture microphone array with 48 microphones. The three measurements were done separately, but all measurements were ensured to be statistically stationary by sampling interval longer than 10 seconds.

III.C.1. Far-Field Microphones

Two lines of microphones were arranged above and below the model. Each line consisted of 8 microphones, 1/4 inch Brüel & Kjær Type 4136, located above and below the midspan of the airfoil model and extended downstream. The line microphones below the model are positioned at different heights from the floor to avoid interaction of the wind tunnel's shear layer with the microphones. Figure 10 shows the arrangement of these far-field microphones. A sampling frequency of 100 kHz was used resulting in 1,000,000 samples collected.

III.C.2. Microphone Arrays

The large aperture microphone array consisting of 96 1/2 inch Linear-X M51 microphones is positioned 0.98 m above the model. Post-processing uses the CLEAN–SC algorithm of Sijtsma.[11] A 10 mm × 10 mm post-processing grid was used to analyze the acoustic source maps. Based on the acoustic source map, the far-field sound spectrum was calculated by local area integration. The far-field sound spectra between the far-field microphone and microphone array are compared.

A small aperture array consisting of 48 1/4 inch Bruel & Kjær Type 4954A microphones was positioned below the model at $z = -1296$ mm. To measure the directivity of the far-field noise, the array was positioned at three different downstream stations at $x = 426$ mm, 770 mm and 1205 mm. All measurements were

Table 3: Far-field microphone placements relative to the center of the nozzle. All measures in mm.

Mic. #	x	y	z
1	0	-850	0
2	298	-875	0
3	498	-892	0
4	647	-905	0
5	747	-914	0
6	896	-926	0
7	1095	-943	0
8	1394	-969	0
9	7	983	8
10	220	983	8
11	485	983	8
12	618	983	8
13	734	983	8
14	1135	983	28
15	1383	983	28
16	1633	983	28

conducted with the center of the array positioned below the midspan of the model. The same signal post-processing for analyzing the results from the large-aperture microphone array was applied for the small-aperture one. The sampling frequency was set to 64 kHz. The setup for both arrays is shown in figure 11.

III.D. Measurement Parameters

The measurement parameters are shown in table 4. Jet noise was measured with $U_\infty = 0\,\frac{\mathrm{m}}{\mathrm{s}}$ and $U_{jet} =$ 170, 200, 230 and $260\,\frac{\mathrm{m}}{\mathrm{s}}$. Baseline measurement provides the reference, where the airfoil's circulation is not controlled. Coanda measurements were performed with free stream velocities of $U_\infty = 30$, 35 and $40\,\frac{\mathrm{m}}{\mathrm{s}}$. Background noise was measured with $U_\infty = 30$, 35, 40, 50 and $60\,\frac{\mathrm{m}}{\mathrm{s}}$ after the airfoil model was removed from the test section.

Table 4: Measurement parameters

Parameter	Magnitude	Notes
U_∞, $[\frac{\mathrm{m}}{\mathrm{s}}]$	0	jet noise measurement
	30, 40, 50	
α_{AWB}, $[^\circ]$	6, 11	
c_μ	0	baseline measurement
	0.066, 0.069, 0.073	Coanda measurements

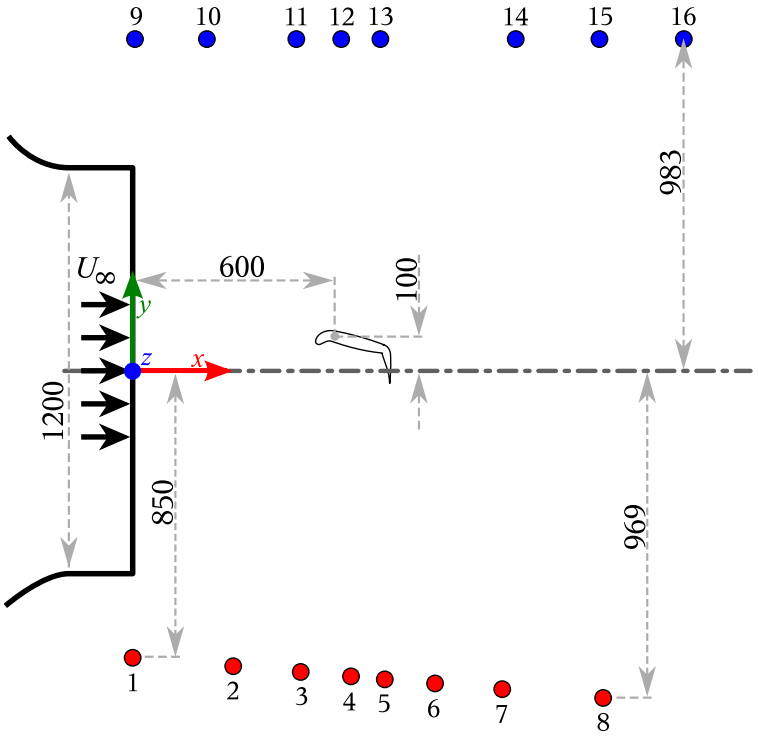

Figure 10: Far-field microphones arrangement with respect to the model installed in the AWB.

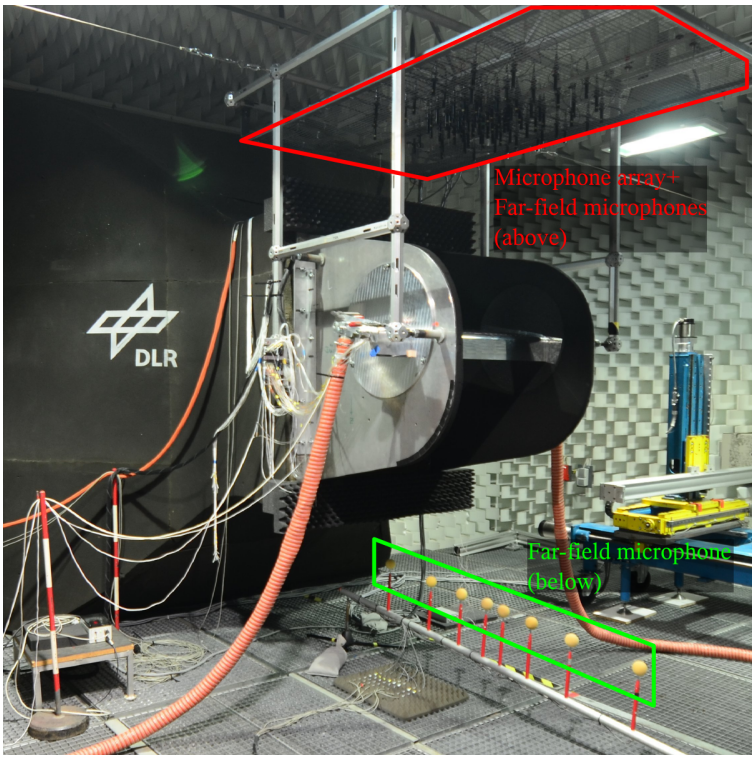

(a)

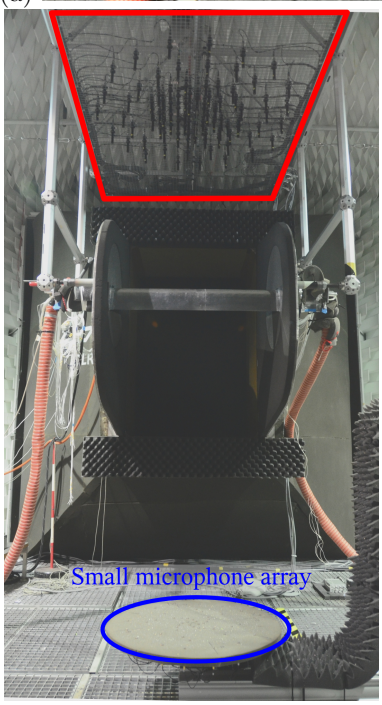

(b)

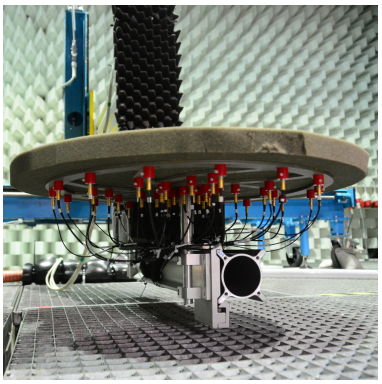

(c)

Figure 11: Acoustic measurements setup in the AWB (a) Far-field microphones and microphone array above the model and far-field microphones below the model, (b) Large and small aperture microphone arrays, (c) Small microphone array.

IV. Results

In the following sections the results from both simulations and experiments regarding the different noise source mechanisms are presented. It has to be noted that for the jet mixing noise a different source model compared to the subsequent simulations is used. Therefore in this 2D setup, the absolute sound pressure levels are not directly comparable. Furthermore, the levels obtained by the simulations are not calibrated to the experimental results. Hence, only qualitative comparison between the different results are feasible.

IV.A. Jet Mixing Noise

IV.A.1. Simulation

The first considered source mechanism is the jet mixing noise that is based on the model formulated by Tam and Auriault.[6] Figure 12 shows a snapshot of the sound pressure field that is radiated. It can be seen that this source produces relatively high frequency noise of more than 10 kHz that mainly radiates downstream and to the top. Below the airfoil a significant shielding effect can be observed, which plays a favorable role considering community noise.

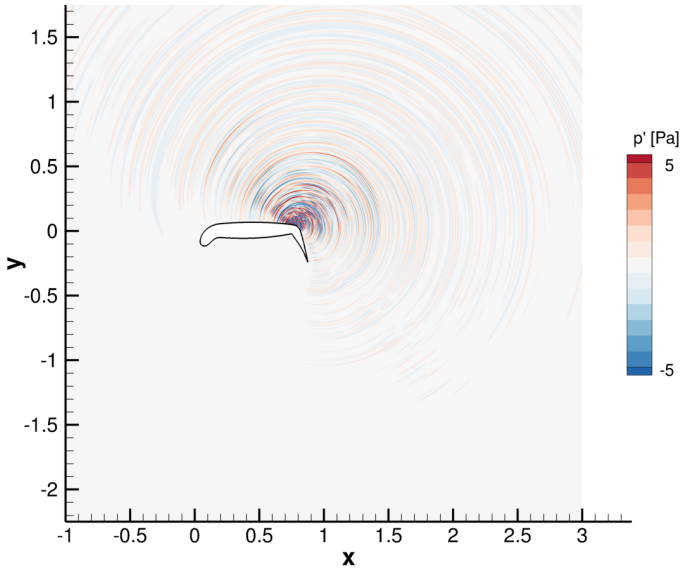

Figure 12: Snapshot of the jet induced sound pressure field.

IV.A.2. Experiment

Jet mixing noise was investigated in the experiments by turning the compressor on while the tunnel was not running. Acquisition of the radiated noise was possible using the far-field microphones as well as the large aperture microphone array positioned above the wing (see figure 11). The resulting spectra for different values of the jet velocity, U_{jet}, are plotted in figure 13. In figure 13a, a comparison is made between the microphone array results and the far field measurement at microphone 12 (e.g. figure 10). Both measurement techniques are found to capture the radiated noise in principle. Of the two techniques, the far field microphones deliver data over a more important frequency range, nominally at high frequencies. The advantage of the microphone array lies in its implicit focusing abilities which will be needed later on when dealing with co-flow situations.

In figures 13b,c two different scalings are applied to the data. Here, we assume $p^2_{rms} \propto U^n_{jet}$ with $n = 6.5$ in figure 13b and $n = 8.0$ in figure 13c. These power exponents are picked because they provide the best collapse of the spectra. The dimensionless frequency axis is calculated using an arbitrary length scale of 1 m and U_{jet}. The results of figure 13b suggest an edge interaction noise source mechanism, mostly important at lower frequencies, which could be originating at the slit lip as proposed by Ffowcs-Williams.[12] He suggested that

the jet exit geometry could affect the noise radiation by an additional component radiating as a fluctuating force dipole source with $p^2_{rms} \propto U^6_{jet}$. Furthermore, Seiner et al.[13] assume $p^2_{rms} \propto U^7_{jet}$, due to a mixing of turbulent jet mixing noise and lip noise, to explain the results of their investigations. In figure 13c, the data scaling indicates that jet mixing noise is dominant at higher frequencies, which is expected due to the small geometric scale of the model slit.

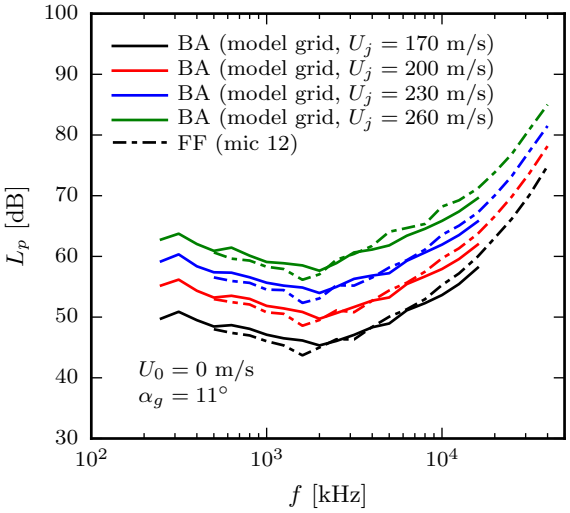

(a) Measured data

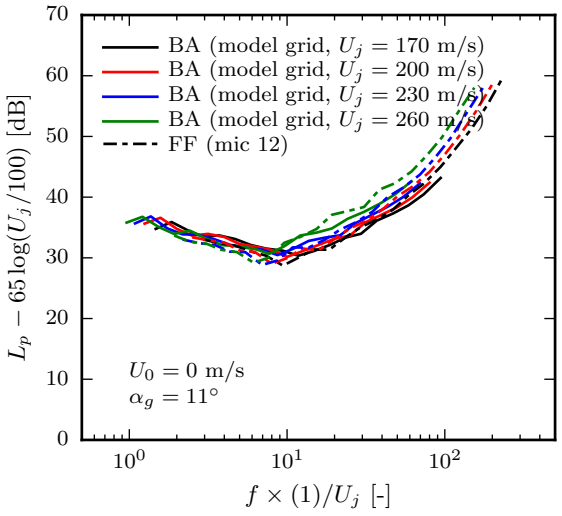

(b) Scaled data, $n = 6.5$

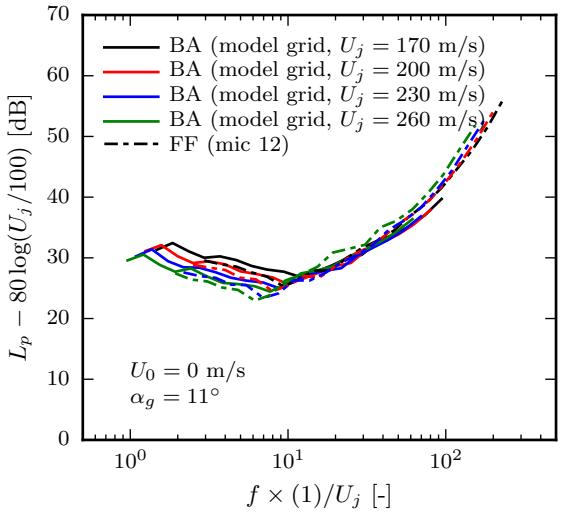

(c) Scaled data, $n = 8.0$

Figure 13: Jet only, scaling assuming $p^2_{rms} \propto U^n_{jet}$, $U_0 = 0\,\mathrm{m/s}$, $\alpha_g = 11°$, BA = large aperture microphone array, FF = far field microphone.

Measurements were also done using a small aperture microphone array traversed on the fly-over line, below the wing (see figure 14a). The corresponding results are plotted in figure 14b. As the microphone is moved upstream, the jet mixing noise contribution is found to diminish due to shielding from the wing, corroborating the simulations. The low frequency part, most probably related to a mixture of TE noise and kink noise (see discussion below), remains mostly constant.

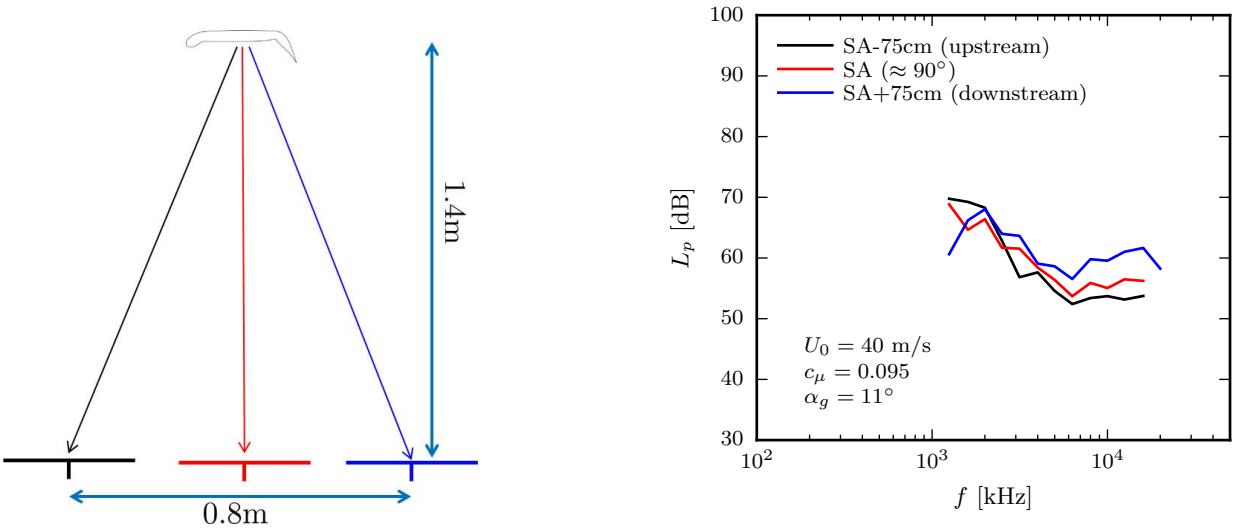

(a) Microphone array positions

(b) Microphone array results

Figure 14: Fly-over line noise radiation directivity. $U_0 = 40\,\mathrm{m/s}$, $\alpha_g = 11°$, $c_\mu = 0.069$. Small aperture array data.

IV.B. Trailing Edge Noise

IV.B.1. Simulation

By avoiding the classic high lift noise from a slat, the noise generated at the trailing edge of the flap is supposed to become a significant acoustic source. The noise radiated from this specific source is illustrated in figure 15 with the source region marked by the blue box. It can be seen that no classic cardioid directivity pattern that would be expected from trailing edge noise is formed. This is most probably due to the highly curved mean flow around the airfoil that leads to a deformation of the emitted sound waves. However, the strongest waves are radiated in upstream direction down from the airfoil. On the one hand, this might be related to the convective amplification and on the other hand to the concave geometry of the airfoil's pressure side, that may act as mirror.

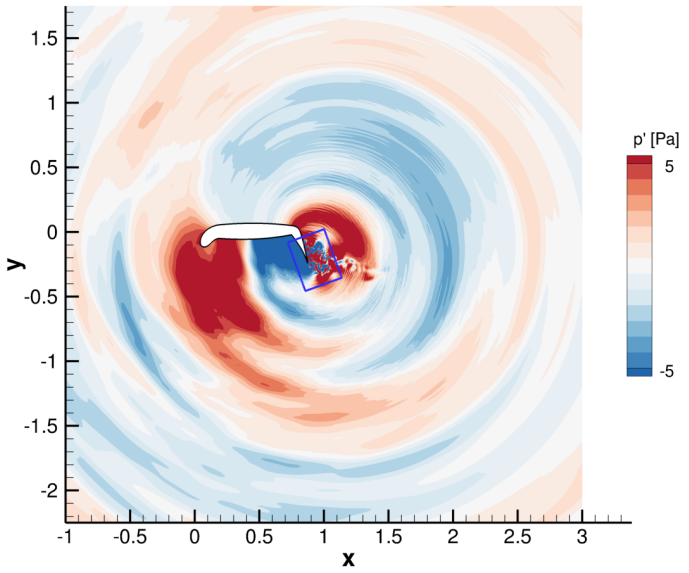

Figure 15: Snapshot of the flap trailing edge noise sound pressure field.

IV.B.2. Experiment

Although the simulations identify the trailing edge (TE) as an important noise generator, it was not clear if TE noise could be isolated experimentally. In the experiment, the quantification of the TE noise contribution was done using the large aperture array (e.g. figure 11). The far field microphones cannot isolate TE noise because of its low level compared to the background noise. Through the application of different potentially noise reducing "treatments" to the wing, TE noise could be successfully reduced. The results of these tests are plotted in figure 16. The solid and dashed black curves correspond to the noise radiation from the reference configuration as measured using the microphone array and far field microphone 12, respectively. In the microphone array data processing the whole of the wing is considered. As already discussed, the agreement between both measurement techniques is excellent. However, they provide a global measure of the noise generated over the complete wing (i.e. region shown by the black dashed rectangle in figure 16a, including the side plate junction region). In the present case, TE noise can only be isolated through a reduction of the area of interest in the microphone array processing (i.e. region shown by the red dashed rectangle in figure 16a). This sub-domain provides the most relevant quantification of TE noise, being free of spurious noise contaminations. In figure 16a, the wing is shown by the dotted black rectangle. In figure 16b, the results obtained using the smaller region of interest are those which cover the reduced frequency range. Four different configurations were investigated, (1) reference configuration, (2) reference + TE brush add-on, (3) reference + kink fairing add-on and (4) reference + TE brush add-on + kink fairing add-on. From the results of figure 16b, the only beneficial treatment is the application of a TE brush, which brings 2 to 5 dB

noise reduction in the range 1.6 kHz $< f_c <$ 10 kHz. Thus TE noise can be reduced through the application of known noise mitigation treatments. One cannot, however, rule out that the results of figure 16 might be a mixture of TE noise and curvature noise (see discussion in the next section). This aspect will be addressed in more details in the final paper.

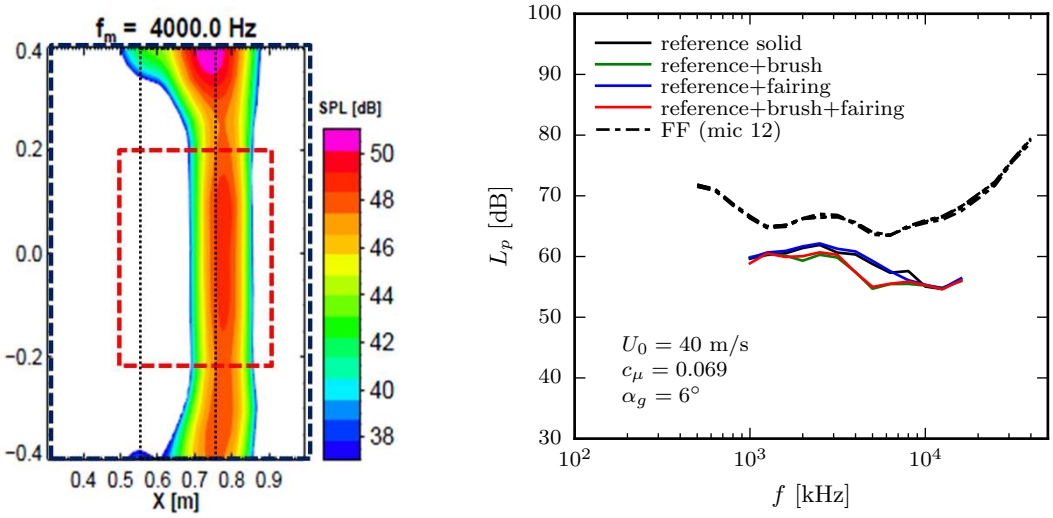

(a) Source map, $f_c = 4$ kHz (b) Measured data

Figure 16: Trailing edge noise reduction, $U_0 = 40$ m/s, $\alpha_g = 6°$, $c_\mu = 0.069$

IV.C. Curvature Noise

A second potential noise source that is based on the interaction of turbulence with the airfoil's geometry is the so-called curvature noise. This occurs, when the turbulent eddies from the suction side boundary layer as well as those from the wall jet are accelerated around the curvature of the flap marked in figure 17 by the red box of the fRPM source region. Compared to the above presented trailing edge noise, this curvature noise is of higher frequency, which is related to the size of the turbulent structures. Furthermore, a similar directivity as for the jet mixing noise can be observed. As before, an effective shielding in upstream down direction can be observed. However, also the main radiation direction is pointing downwards. Hence, the shielding is less effective as for the jet mixing noise when considering community noise. In terms of sound pressure levels, the curvature noise is of a similar magnitude as the trailing edge noise. Other than for the jet mixing noise, this comparison is supposed to be valid as the same source modeling for the trailing edge and the curvature noise is used.

IV.D. Flap Kink Noise

IV.D.1. Simulation

The last possible considered noise source location is found on the pressure side of the airfoil in the region of detached flow at the flap, shown by the green box in figure 18. The radiated sound pressure levels are of more than one order of magnitude smaller than for the trailing edge noise and the curvature noise. Hence, even if this source mainly radiates in downward direction, it does not seem to be a significant acoustic source. This observation is also related to the turbulence intensity that is lower than at the trailing edge or the jet region.

IV.D.2. Experiment

As already discussed in section IV.B when considering the trailing edge noise, potentially noise reducing elements were applied to the airfoil. One of them was a fairing to fill the flap kink. Thereby, the flow separation should at least be reduced, which is supposed to have a direct impact on the emitted noise. As shown on figure 16b, the fairing has no detectable effect on the measured spectra. This might be an

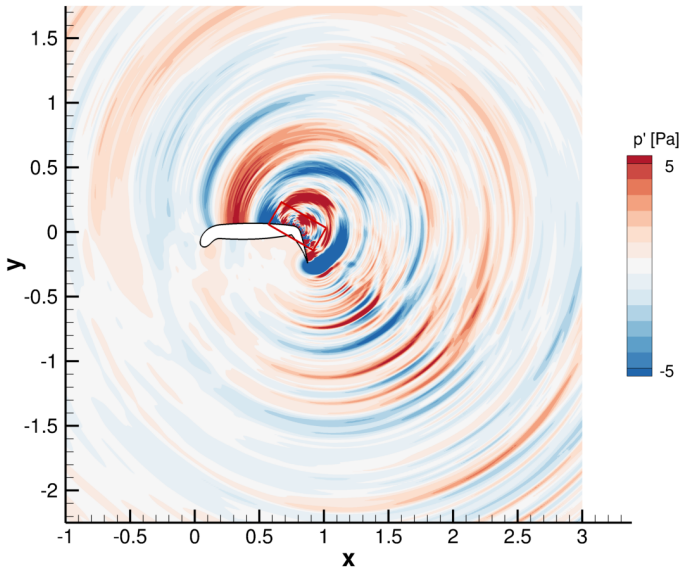

Figure 17: Snapshot of the curvature noise sound pressure field.

indication that the noise emitted from the separation is indeed no dominant source mechanism, as suggested by the numerical result.

V. Summary and Outlook

In the present abstract the numerical and experimental analysis of noise radiated from an airfoil with circulation control is addressed. Despite the fact that two different configurations with deviating extensions of the flap are considered, valuable insights to the acoustic source mechanisms on such high lift airfoil are provided. The simulations are used to do an acoustic breakdown to single sources on the airfoil, as jet mixing noise, trailing edge noise, curvature noise and flow separation noise. It was found that for the downward facing radiation direction, which is of special interest considering community noise, trailing edge noise and curvature noise are the dominant contributors. On the experimental part of the work, for now mostly analysis of the velocity scaling is provided. Here, two different regimes are identified when considering jet noise. In the low-frequency domain presumably jet-nozzle interaction becomes dominant while for higher frequencies jet mixing noise is expected to be the driving source mechanism. Furthermore, a first approach to noise reduction techniques is made. Thereby, it was shown that brushes applied to the trailing edge of the flap reduce the emitted noise for frequencies in the range of 2-10 kHz. This supports the assumption gained from the simulations, that trailing edge noise might in fact be a considerable noise source mechanism on such circulation-control airfoils.

In the future the results of this work may serve as a basis to come up with efficient noise reduction techniques, such as trailing edge devices or changes in the design of the flap that can be tested both numerically and experimentally.

For the final paper, more simulations will be run with the configuration from the experimental tests. With these, a more detailed analysis of the data will be possible. The aim is to get a better understanding of the weighting of the different contributing noise sources. Plus, a more detailed analysis of the experimental data will be carried out to compare to the numerical findings.

VI. Acknowledgement

Financial support is provided by the German Research Foundation (Deutsche Forschungsgemeinschaft, DFG) in the framework of the Sonderforschungsbereich 880. Computational resources are provided by Ger-

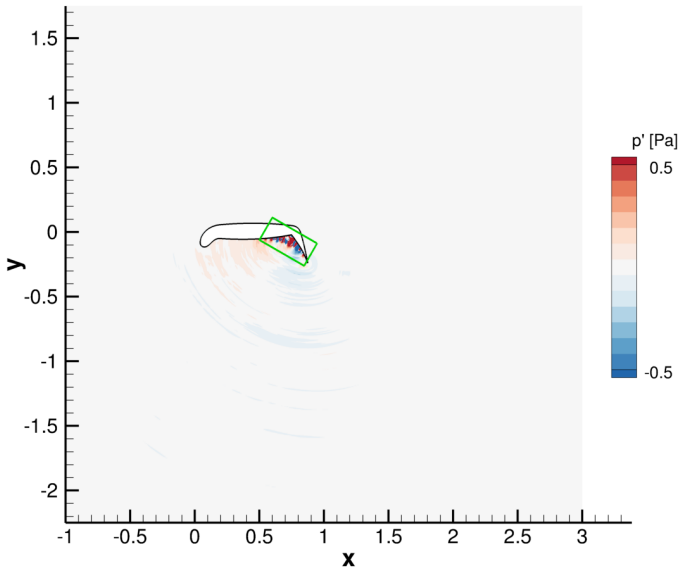

Figure 18: Snapshot of the flap kink detached flow noise sound pressure field.

man Aerospace Center (Deutsches Zentrum für Luft- und Raumfahrt e.V., DLR), Institute of Aerodynamics and Flow Technology.

References

[1]Coanda, H., "Procédé de propulsion dans un fluide," 1932.

[2]Pfingsten, K. C. and Radespiel, R., "Experimental and numerical investigations of a circulation control airfoil," Tech. rep., 2009.

[3]Loth, J. L., "Advantages of combining BLC suction with circulation control high-lift generation," *Application of circulation control technology, Progress in Astronautics and Aeronautics*, Vol. 214, pp. 3–21.

[4]Pott-Pollenske, M. and Pfingsten, K. C., "Aeroacoustic Performance of an Airfoil with Circulation Control," AIAA Paper 2010-3881, 2016.

[5]Howe, M. S., "Analytical Study of the Noise Generated by a Coanda Wall Jet Circulation Control Device," Final Report AM 00-004, 2000.

[6]Tam, C. K. W. and Auriault, L., "Jet Mixing Noise from Fine-Scale Turbulence," *AIAA Journal*, Vol. 37, No. 2, pp. 145–153.

[7]Neifeld, A., Boenke, D., Dierke, J., and Ewert, R., "Jet Noise Prediction with Eddy Relaxation Source Model," AIAA Paper 2015-2370, 2015.

[8]Ahuja, K. K., Sankar, L. N., Englar, R. J., Munro, S. E., Li, Y., and Gaeta, R. J., "Application of Circulation Control Technology to Airframe Noise Reduction," GTRI Report A5928/2003-1, 2003.

[9]Rossian, L., Faßmann, B. W., Ewert, R., and Delfs, J. W., "Prediction of Porous Trailing Edge Noise Reduction Using Acoustic Jump-Conditions at Porous Interfaces," AIAA Paper 2016-2920, 2016.

[10]Pott-Pollenske, M. and Delfs, J., "Enhanced Capabilities of the Aeroacoustic Wind Tunnel Braunschweig," *14th AIAA/CEAS Aeroacoustics Conference (29th AIAA Aeroacoustics Conference)*, , No. May, 2008, pp. 1–11.

[11]Sijtsma, P., "CLEAN based on spatial source coherence," *International journal of aeroacoustics*, Vol. 6, No. 4, 2007, pp. 357–374.

[12]Williams, J., "Some open questions on the jet noise problem," Tech. rep., BOEING SCIENTIFIC RESEARCH LABS SEATTLE WASH FLIGHT SCIENCES LAB, 1968.

[13]Seiner, J. M., Manning, J., and Ponton, M., "Acoustic properties associated with rectangular geometry supersonic nozzles," *Thermophysical Aspects of Re-entry Flows*, 1986.